RESEARCH ARTICLE | AUGUST 04 2025

Plasmonic heating, thermoelectric response, and thermal emission in titanium nitride nanowires

Ken W. Ssennyimba ; Shusen Liao ; Yunxuan Zhu ; Tanner J. Legvold ; Dale T. Lowder ; Karthik Pagadala ; Alexandra Boltasseva ; Vladimir M. Shalaev ; Douglas Natelson

APL Mater. 13, 081108 (2025)
https://doi.org/10.1063/5.0276431
CHORUS

Plasmonic heating, thermoelectric response, and thermal emission in titanium nitride nanowires

Cite as: APL Mater. 13, 081108 (2025); doi: 10.1063/5.0276431
Submitted: 17 April 2025 • Accepted: 19 July 2025 •
Published Online: 4 August 2025

Ken W. Ssennyimba,[1] Shusen Liao,[1] Yunxuan Zhu,[3] Tanner J. Legvold,[2] Dale T. Lowder,[2] Karthik Pagadala,[4] Alexandra Boltasseva,[4] Vladimir M. Shalaev,[4] and Douglas Natelson[2,5,6,a)]

AFFILIATIONS

[1] Applied Physics Graduate Program, Smalley-Curl Institute, Rice University, Houston, Texas 77005, USA
[2] Department of Physics and Astronomy, Rice University, Houston, Texas 77005, USA
[3] Department of Mechanical Engineering, University of Colorado-Boulder, Boulder, Colorado 80309, USA
[4] Elmore Family School of Electrical and Computer Engineering, Birck Nanotechnology Center, Purdue University, West Lafayette, Indiana 47907, USA
[5] Department of Electrical and Computer Engineering, Rice University, Houston, Texas 77005, USA
[6] Department of Materials Science and NanoEngineering, Rice University, Houston, Texas 77005, USA

Note: This paper is part of the Special Topic on Photothermal Materials.
[a)] **Author to whom correspondence should be addressed:** natelson@rice.edu

ABSTRACT

Unlike noble metals, refractory plasmonic materials can maintain resilient and attractive optical properties even at comparatively extreme temperatures and high current densities. One refractory plasmonic material of interest is TiN, which exhibits an extremely high melting temperature of about 3000 K and noble-metal-like optical properties in the visible and near-infrared regime. Using lithographically fabricated TiN nanowires and leveraging their ability to host plasmon modes, we have examined plasmonic photothermal heating and photothermoelectric response whose anisotropy and magnitude depend on the width of the nanowires. The photothermoelectric response is consistent with changes in the Seebeck coefficient where the wire fans out to wider contact pads. Upon electrically biasing the structures, Joule heating of the TiN wires can produce detectable thermal emission within the visible and near-IR range, with emission intensity growing rapidly with increasing bias. This emission is consistent with local temperatures exceeding 2000 K, as expected from a finite element model of the Joule heating.

INTRODUCTION

Photothermal effects in nanostructures are an active research topic owing to diverse applications in optical detection, sensing, catalysis, and even cancer therapy.[1–3] Photothermal response involves the maximal absorption of light and its subsequent conversion into heat in many systems, including organic materials (polymers[4]) and a variety of inorganic materials (such as semiconductors and plasmonic materials[5,6]). Photothermal effects are prevalent in plasmonic materials because geometrically tunable plasmon resonances in optical absorption contribute to the optical heating of the charge carriers and the lattice. An exceptional response results from strong dipole absorption moments facilitated by the hosted surface plasmon resonances in these materials. These resonances originate from coherent electronic oscillations on the metallic surface and play an essential role in determining the optical properties of the structure. Plasmon resonances in these materials define the optimal operational wavelengths of optically and/or electrically driven nanostructures by shaping their emission spectra and polarization.[7,8] These features are crucial for

applications that involve unique light–matter interactions, such as polarization-sensitive tomography[9] and sensing.[10]

Photothermal response has also proven useful for photodetection through bolometric changes in device resistance[11–13] and photothermoelectric generation of an open-circuit photovoltage (OCPV).[14–16] These features fuel the research interest in these efficient photon-to-heat energy converters for diverse applications. As such, plasmonic materials such as noble metals and some conducting oxides[17–19] have been extensively studied owing to their response to photothermal heating in the visible and near-infrared regimes. A challenge for these materials is the need to guarantee efficient energy conversion for applications requiring high operational temperatures and/or high current densities. Nanostructures of non-refractory materials can undergo geometric deformations at relatively low temperatures, leading to poor stability and drastic changes in the electromagnetic absorption properties under high temperatures and current densities.

Titanium nitride is an inexpensive alternative to the relatively costly noble metals, possessing a refractory ceramic nature with a dielectric function favoring plasmonic response in the red and near-infrared, such as gold.[20,21] The ability of TiN to absorb efficiently within the biological transparency window has made it attractive for photothermal therapy treatments.[22] The biocompatibility and relatively high melting temperature, even for nanostructured forms, have fueled its integration and development in various nanostructure-based photothermal applications.[23]

TiN has been employed in nanoparticle form[24] as well as in metasurfaces[25] for photothermal applications. Schramke *et al.* recently studied the photothermal response of titanium nitride nanocrystals fabricated via a nonthermal plasma route.[24] TiN metastructures have also been studied as candidate plasmonic materials for solar harvesting.[26] These features motivate exploring the photothermal responses of other TiN nanostructures. Metallic TiN nanowires have proven to be easily fabricated, exhibit good tunability, show complementary metal–oxide–semiconductor (CMOS) compatibility, and have excellent plasmonic resonances that can be tailored for diverse photothermal applications. However, direct electrical detection of photothermal effects in individual TiN nanostructures remains comparatively unexplored, as do investigations of optical emission from electrically driven TiN nanostructures.

In this work, we present studies of the photothermal response of individual TiN nanowires. Measurements of resistance as a function of incident polarization show clear evidence of an expected transverse dipolar plasmon resonance, consistent with finite element modeling of the optical response. Photothermoelectric measurements reveal that it is possible to create optically excitable single-material thermocouples from TiN that produce readily measurable open-circuit photovoltages (OCPVs) when illuminated. The refractory properties of TiN mean that resistively heated nanowires can reach electron temperatures sufficient to emit in the visible. While emission spectra in the example devices here are modified by interference effects involving the underlying SiO_2, analysis based on a normalization approach finds a Boltzmann-like energy dependence with an effective temperature comparable to that found in simulations.

EXPERIMENTAL AND THEORETICAL METHODS

Fabrication of the plasmonic TiN nanowire (NW) bowtie structures

2 μm thick SiO_2/Si wafers were used as substrates for depositing 100 nm TiN films. The TiN films were grown using DC reactive magnetron sputtering (PVD Products) at a temperature of 800 °C. A 99.995% pure Ti target of 2-in. diameter and a DC power of 200 W were used for the process. The distance from the target to the source is kept at 20 cm to ensure uniformity. The chamber is pumped down to 3×10^{-8} Torr before deposition to prevent oxygen contamination and backfilled to 5 mTorr with argon during the sputtering process. The Ti target is initially sputtered in an argon plasma for 2 min with a power of 200 W to clean the target surface. The TiN films were then deposited using an argon–nitrogen mixture flowing into the chamber at the rate of 1 SCCM/18 SCCM, along with a substrate rotation speed of 5 rpm. Clean TiN-coated wafers were then spin-coated with negative-tone resist (maN-2403), baked at 100 °C for 90 s, and subtractively patterned using standard e-beam lithography and revealed by rinsing the e-beam exposed resists in an aqueous-alkaline-based (ma-D 525) solution. The sample was then structured by reactive ion etching (RIE) to have an array of TiN NWs of widths ranging from 50 to 500 nm, a range designed to span the widths expected to produce a transverse plasmon resonance that could be excited by incident 785 nm wavelength illumination. The RIE was done using a gas mixture of gas ratios of sulfur hexafluoride (SF_6) and argon (Ar) with flow rates of 30 and 18 SCCM, respectively. The pressure, rf power, and bias DC power were 10 mTorr, 90 W, and 175 V, respectively. The typical etching lasted about 4.5 min. The residual resist on top of the NWs was stripped using acetone, and the samples were then rinsed in IPA and blow-dried with air. The resulting TiN nanowire bowtie structures were then connected to large photolithographically defined electrode pads comprising metal layers of 5 nm Ti for adhesion underneath 50 nm gold (Au). The photoresist was stripped in acetone. The resulting sample, comprising 24 devices with a common ground, was connected to a larger chip carrier using Au wires by wire bonding. Devices were then immediately transferred to a Montana Instruments vacuum cryostat for measurements. For the measurement of each individual nanowire, the other nanowires on that same substrate were left floating.

Characterization

The OCPV and photothermal heating measurements were done using setups described in previous studies.[11,14] For the heating measurements, the devices were biased at 5 mV dc. A linearly polarized 785 nm CW laser was the excitation source. A mechanical chopper rotating at 270 Hz) (a period much slower than the associated thermal timescales of the plasmonic structures[27–29]) modulated the laser, while a half-wave plate and polarizer controlled its intensity. The laser beam was focused through a high NA objective (Nikon 50×, NA 0.7) to produce a spot diameter of full width half-maximum (FWHM) 1.8 μm on the sample surface. A telescopic lens was used to raster scan the laser spot on the sample surface. OCPV and photocurrent maps were both measured using a lock-in amplifier synced to the chopper frequency and an SR560 voltage amplifier or an SR570 current amplifier, respectively.

For the thermal emission measurements, the NWs biased by the Keithley 2400 source meter emit photons, which are collected by the high NA objective and directed to an optical spectrometer (Horiba iHR 320/Synapse CCD) for measurement. All the light emission results in this work were corrected for the spectral response of free space optics and the silicon charge-coupled detector (CCD) in the spectrometer.

Optical and thermal simulations

We performed finite element simulations to compare with our experimental results using COMSOL Multiphysics version 6.1. For the optical simulations, plane waves of various intensities normally incident on the metallic nanowire induce plasmonic excitations. The measured optical properties of our TiN films were used to calculate absorption cross sections for varying nanowire widths and at a fixed incident wavelength of 785 nm. The results were used to optimize the nanowire width for plasmonic absorption and fed into a thermal model to calculate the power dependency of the laser heating for the nanostructures. Calculated absorption cross sections for both polarizations were used to determine the dominant modes in the geometry-optimized TiN NW. The ΔT vs laser power plots were obtained from simulations implemented in $3D$ using Heat Transfer in the Solids and Electromagnetic Waves domains physics modules. The Joule heating simulations were performed simultaneously using the electric currents and the heat transfer module. Two-probe techniques were used to measure the electrical resistivity used for the modeling.

As verified by prior studies with Pt NWs,[30] the contribution of the contact pads is negligible, so we reasonably truncate them in the thermal model. In addition, the thickness of the Si substrate is truncated for computational efficiency because the Si substrate is approximated to be uniformly held at the sample holder temperature, and the thermal conductivity of Si (148 W/mK) is much higher than that of the amorphous SiO_2 (0.6 W/mK) substrate. This is in agreement with previous studies, which suggest that the low thermal conductivity of SiO_2 constrains most of the heat flow to the etched TiN structure (which thermally conducts at about 19 W/mK). This also validates our device fabrication design since it minimizes heat wastage to untargeted regions. This modeling aims to understand if the lattice of the electrically biased TiN nanowire gets heated to electron temperatures sufficient to produce the observed thermal emission. The electrical properties used in this model are adopted from our resistance vs temperature measurement shown in Fig. 1(c).

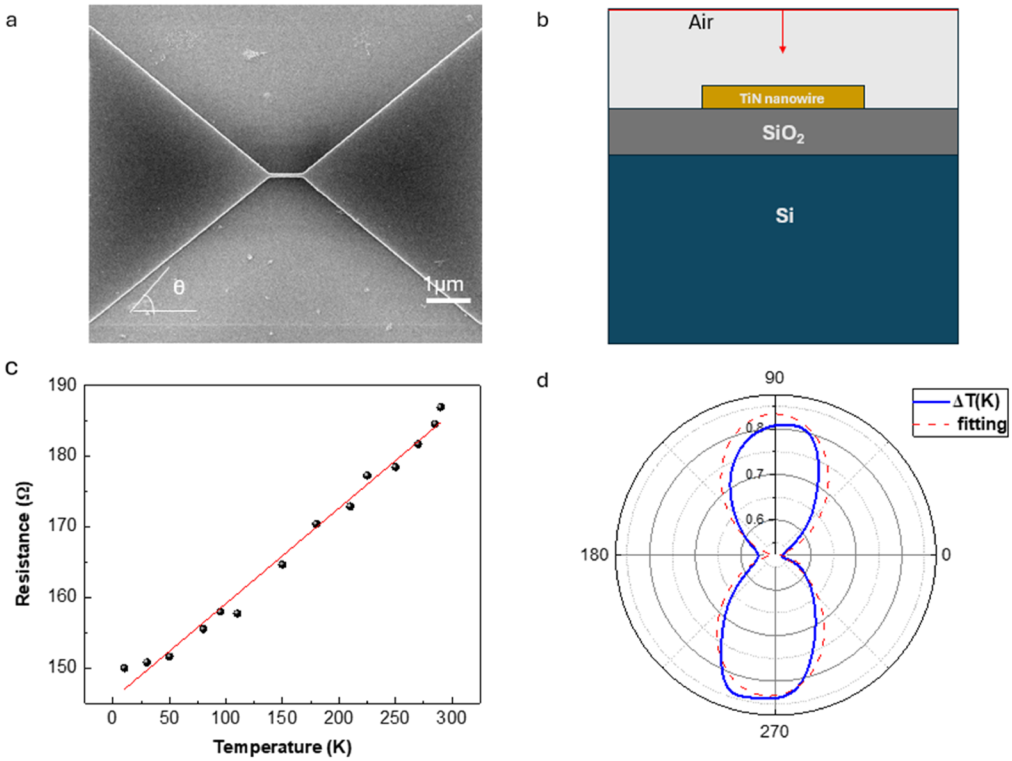

FIG. 1. (a) Micrograph of etched nanowire structure. (b) Schematic cross section diagram of device geometry used in finite element simulations (geometry not to scale). The nanowire direction is in/out of the page. The red arrow indicates the incident plane wave, with polarization in the plane of the page. (c) Typical resistance as a function of temperature for TiN nanowire. (d) Polarization dependence of effective temperature change, including fit to $A + B\cos^2\theta$ for a sample at 180 K on a 2 μm thick SiO_2 substrate.

RESULTS AND DISCUSSION

Plasmonic resonances and photothermal heating in TiN nanowires

We consider etched nanowires connected to large contact leads, as shown in Fig. 1(a). The resistance of these structures is dominated by the nanowire constriction. Incident light absorbed by the TiN increases the local temperature, which leads to an increase in the device resistance proportional to the incident optical power. This photothermal resistance change, measured using a lock-in amplifier synchronized to the chopper that modulates the incident light, can be converted into a temperature change via the experimentally determined resistance as a function of temperature, $R(T)$ [Fig. 1(c)].

We conducted temperature (T)-dependent resistance (R) measurements on 11 individual TiN NWs. A typical R vs T relationship for our devices is illustrated in Fig. 1(c). The R vs T plots are nonlinear for all devices, with smaller positive local slopes recorded for colder temperatures below 40 K, as expected for the freezing out of phonon scattering of the carriers.[31] At warmer temperatures, the R vs T plots have larger positive slopes, implying higher temperature coefficients of resistance. We performed all heating experiments with substrate temperatures held at 180 K, where the typical $\frac{dR}{dT}$ ranges from 0.1 to 0.35 ΩK^{-1} extracted from a temperature range of 80–300 K to calculate the extent of the plasmonic heating.

Temperature changes ΔT due to small variations in the resistance of the NW at a fixed bias voltage V_{dc} can be inferred from Ohm's law and the chain rule decomposition of $\frac{dR}{dT}$. With these, the plasmonic heating can be quantified using a derived expression,

$$\Delta T = -\frac{R^2 \delta I}{\frac{dR}{dT} V_{dc}}.$$

Here, δI is the optically induced change in current. For the transverse (θ=90°) polarization of the heating laser beam, ΔT was deduced experimentally to be in the range of 0.1–1.1 K, depending on incident power.

COMSOL simulations [schematic shown in Fig. 1(b)] of an infinitely long TiN strip show a clear transverse, dipolar plasmon resonance when the incident radiation is polarized transverse to the nanowire. This is reminiscent of what was previously observed in Au nanowires.[32]

Our simulation results [Fig. S2(a)] indicate that the width-normalized absorption sharply decreases for wider widths. Therefore, it is reasonable to neglect the absorption contribution from the wider portions of the fan-out region of our bowtie devices, allowing for the simulation of a simplified 2D model depicted in Fig. 1(b). We would like to emphasize that, in this model, the nanowire is considered infinitely long, extending in/out of the page. The polarization dependence of this resonant contribution to the absorption is clearly shown in Fig. 1(d). With insight from previous work done on individual plasmonic nanorods,[33] the inferred temperature change is fit to the form $A + B\cos^2\theta$, where θ refers to the polarization angle, which is zero when the incident beam is polarized along the NW length. The parameter B is proportional to the transverse resonance contribution, while A originates from the isotropic, direct optical absorption of the TiN. The transverse resonance depends on both the dielectric function of the TiN and the geometry of the wire.

The interaction strength between the polarized light and the NW-hosted plasmons is highly width-dependent, as expected when accounting for a transverse dipolar plasmon resonance of the NW. For NWs of varying widths, the plasmonic contribution to the heating response shows a clear trend with wire width, with weaker cosine-squared components for wires deviating from 186 nm in width [Fig. 2(a)].

Figure 2(b) shows the theoretical expectation of the steady-state induced temperature rise in the nanowire's hottest spot as a function of resonant absorbed laser power at a fixed incident wavelength of 785 nm and a wire thickness of 120 nm as a function of wire width. The absorption, calculated using the experimental dielectric function, is incorporated with the power of the heat source to calculate the temperature rise due to the laser heating. The slight disagreement between the measured and calculated values most likely results from experimental conditions not accounted for in the simulation, for example, surface roughness and the influence of temperature on the plasmon resonances. Consistent results for the geometry dependence of the transverse resonance are seen across two different fabrication batches of nanowires [different symbols in Fig. 2(c)]. We define the plasmonic anisotropy ratio as the ratio of the resonant to the non-resonant temperature rises ($AR \equiv \Delta T(\theta = 90°)/\Delta T(\theta = 0°)$). The experimentally determined and simulated anisotropy ratios follow a similar trend, emphasizing the geometry dependence of the photothermal response in the NWs. The experimental AR range is smaller than the theoretical calculation based on expected TiN optical properties. The fabricated nanowires likely have poorer resonances and larger (polarization-independent) direct absorption from geometrical imperfections and disorders arising from the fabrication process.

This anisotropy, resulting from the polarization-dependent plasmon absorption, can enable rational design of photothermal heaters or on-chip bolometric photodetectors. Normalizing the calculated absorption by the width of the nanowires allowed for the inference of the geometrical contributions to the absorption cross section [Fig. 2(d)]. With this, the theoretical AR was calculated. As expected, nanowires with widths far away from the plasmonic resonant peak exhibited smaller ARs than those with widths (150–250 nm) close to the plasmon peak.

Photothermoelectric response

Single metal thermocouples have been demonstrated in different conductive materials.[34,35] If the heating of these devices is through optical absorption and plasmonic resonances of the metal nanostructures that tune the absorption, it is possible to use such devices as polarization-sensitive photodetectors.[15] The underlying physics of these systems is a systematic change in the Seebeck coefficient, S, that correlates with the physical dimensions of the metal nanostructure. Thus, a wire with an abrupt change in width w can function as a thermocouple, with the wider and narrower wire segments having differing $S(w)$.

Thick TiN thin films are known to have metallic properties owing to thickness-dependent improvement of grain sizes and surface roughness.[31,36] As such, a possible explanation for such geometry dependence of S in our films is boundary scattering and its effect on the mean free path and, thus, the energy-dependent

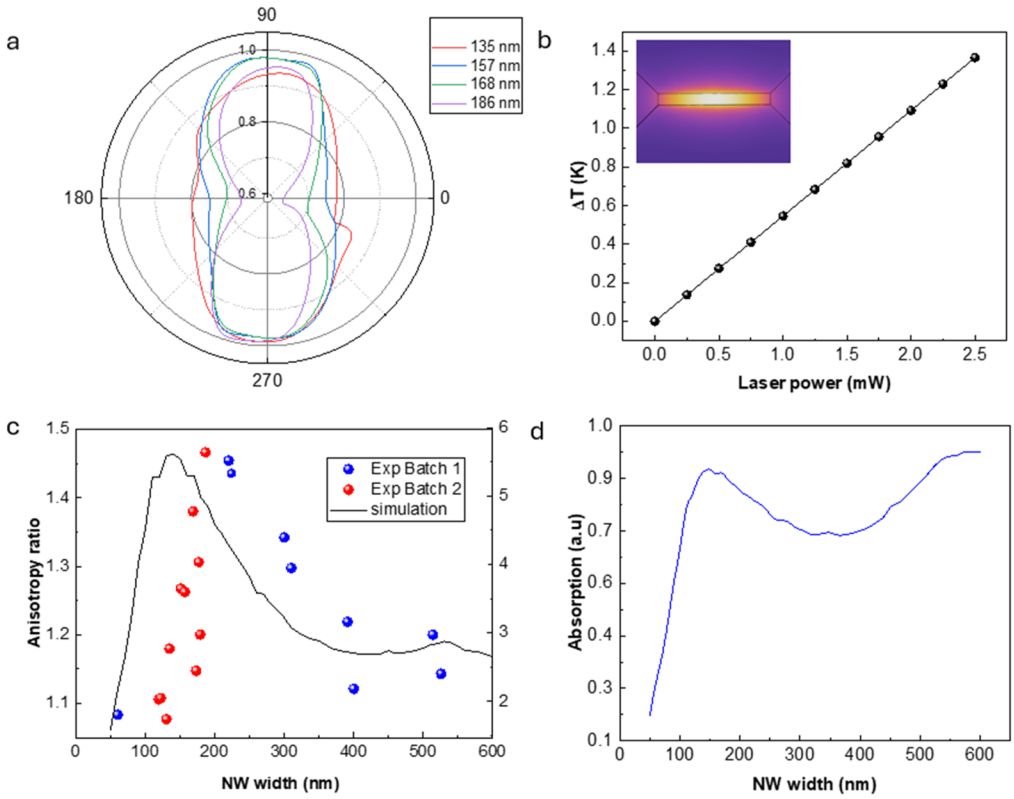

FIG. 2. (a) Polarization-dependence of temperature change for different wire widths when the laser illuminates the TiN NW. (b) Finite element method (FEM) simulation of the induced maximum temperature rise in the central NW (inset) as a function of incident laser power for a fixed photon wavelength and a NW width of 785 and 120 nm, respectively. (c) The magnitude of the plasmonic anisotropy ratio due to heating as a function of wire width, showing consistency across two batches of samples. The right and left axes represent the measured and the calculated ARs, respectively. (d) Simulated absorption normalized by the widths of TiN nanowires comparing different widths under 785 nm laser illumination.

conductivity that appears in the Mott expression,[37] $S = \frac{\pi^2}{3}\frac{k_B^2 T}{e}\frac{\sigma'}{\sigma}$, in which k_B and e have their usual meaning, and the ratio $\frac{\sigma'}{\sigma}$ is the electrical conductivity term representing the details of scattering. Seebeck mapping measurements in metal films, however, have shown local variations in S in the absence of geometric changes,[38] and experiments on highly crystalline nanowires show that local strain can alter S, leading to OCPVs under illumination.[39]

TiN nanowire constrictions, as in Fig. 1(a), show a clear OCPV response as a function of laser position, as shown in Fig. 3(a). Upon illumination of the NW at its center, the measured OCPV is zero due to the symmetry of the geometry and temperature profile. As in similar bow-tie designs made from evaporated Au films,[14,38] there is a maximum in OCPV when the laser is focused on the junction between the nanowire and the fan-out to larger contact pads. As expected for a photothermal effect, the magnitude of the OCPV is linear in the incident optical power [Fig. 3(b)]. At fixed optical power, the OCPV is maximized when the incident polarization is transverse to the nanowire, consistent with the plasmon resonant heating discussed above. As with the plasmonic heating [Fig. 1(d)], illuminating the NW with a transverse resonance gives the largest heating response owing to the dipolar nature of the transverse plasmon mode. This heating response yields the largest temperature difference between the heated location and the ambient temperature ends of the structure. As such, OCPV is the largest when the NW is heated with transverse polarization [Fig. 3(c)].

We measured the OCPV for 22 individual continuous nanowires of the same width, with the majority of the devices having similar $|\Delta V| < 0.2$ μV/mW, as shown in Fig. 3(d). The small $|\Delta V|$ is attributed to the absence of nanogaps or broken symmetries in the NWs. In such NWs, the origin of the measured ΔV is widely accepted to be the photothermoelectric (PTE) effect due to changes in S when the nanowire fans out to larger contacts. The changes in Seebeck response can originate from either boundary scattering affecting the energy-dependent mean free path of charge carriers (Mott formula) or internal stresses in the TiN film that could arise from the film deposition and etching processes. From our measurements, we estimate a modal ΔV from Fig. 3(d), and together with the resonant temperature gradient from Fig. 1(d), we estimate the difference between the Seebeck coefficient of the fan-out electrode (S_f) and that of the nanowire (S_w), ΔS, to be 0.31 μV/K.

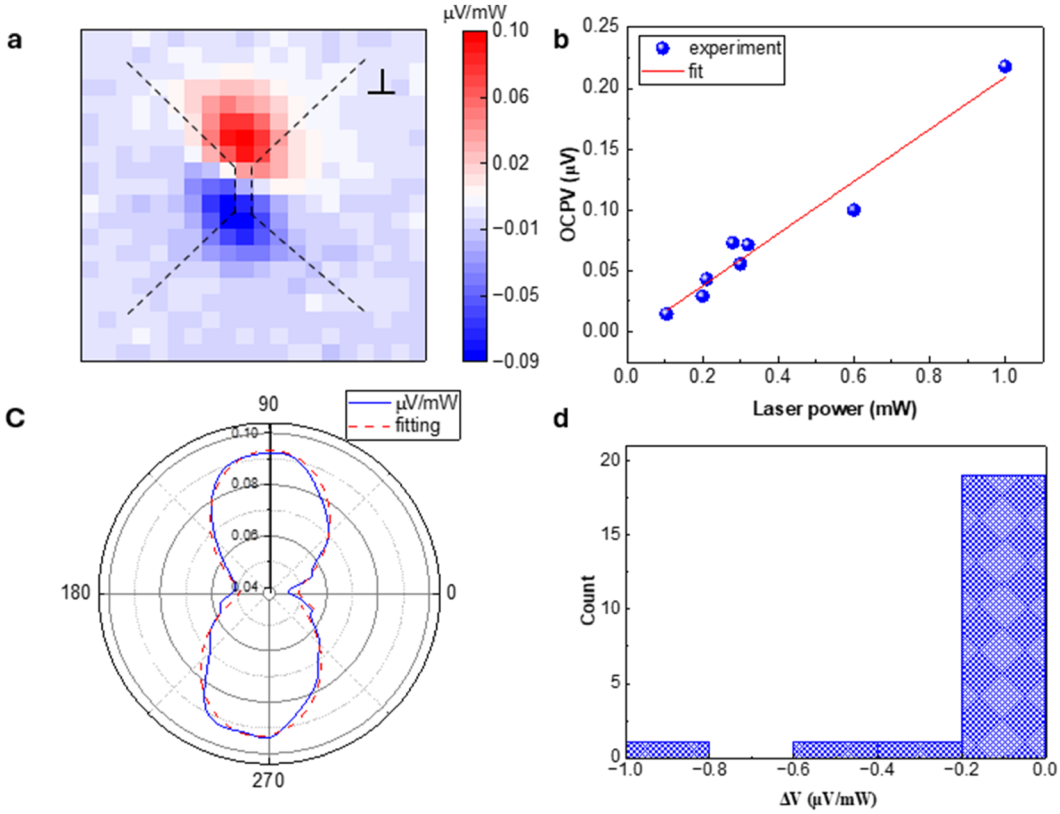

FIG. 3. (a) Map of open-circuit photovoltage (OCPV) as a function of laser position. Dashed lines guide the eye to the outline of NW geometry superimposed on the map. The nanowire width is ~150 nm. (b) OCPV as a function of incident optical power with the laser focused on the location of greatest response. (c) OCPV as a function of incident polarization at a substrate temperature of 180 K. (d) Distribution of maximum OCPV magnitude across multiple geometrically identical devices at a fixed incident power of 2.5 mW.

In the device connection diagram shown in Fig. S1(a), the left boundary is grounded while the right is isolated. This wiring setup is crucial for accurate inference of the sign of ΔS. When heated away from the center of the nanowire geometry, the OCPV color map exhibits two regions of opposite polarity. However, this does not impact the inferred sign of ΔS. To elucidate this, consider the region where the OCPV is negative. The induced temperature difference between the laser spot position and the ambient is positive. Given that our TiN films have a negative Seebeck coefficient of $-6\ \mu$V/K, the relationship $\Delta V = -\Delta S \Delta T$ necessitates a positive ΔS, consistent with our findings. A similar analysis with the positive ΔV region supports the same sign of ΔS, as the sign of the temperature gradient is reversed. The positive sign of ΔS implies that $|S_w| > |S_f|$, which is explained by enhanced scattering effects that are more dominant in the wire than the fan-out. Comparable results have been seen in similar experiments with Au NWs. Our shorter devices ($\leq 1\ \mu$m) exhibited a resolvable PTE response with a few outliers in the magnitude of the response, raising questions about whether this response is due to strain in the NWS. The PTE response of NWs is longer than the diameter of the beam spot and serves as a confirmatory probe for strain-induced Seebeck changes in the nanowires. Unlike gold, where long wires show spatially variable PTE voltage along the nanowire due to non-uniform strain distribution,[38] longer TiN devices (~10 μm) do not exhibit a measurable PTE response when illuminated far from the fan-outs. This is consistent with uniform rather than inhomogeneous stress in the longer wires. This result is consistent with a sharp decrease of strain with increasing thickness in TiN thin films,[40] implying very low strain levels in our 100 nm thick NWs, leading to an unresolvable PTE response. Consequently, it was challenging to place a limit on the contribution of strain to the measured PTE voltages using established techniques that have proven effective for Au.

Thermal light emission

Thanks to the refractory nature of TiN, it is possible to use such TiN nanowires as resistively heated, nanoscale thermal light sources. We employ three-dimensional finite element modeling to qualitatively examine heat dissipation during thermal emission. As shown in Figs. 4(a) and 4(b), for reasonable values of device dimensions, electrical properties, and thermal properties, the simulations show that comparatively modest currents are sufficient to heat the nanowire region far above ambient conditions (180 K for the experiments at hand). The lattice temperature decreases sharply along the

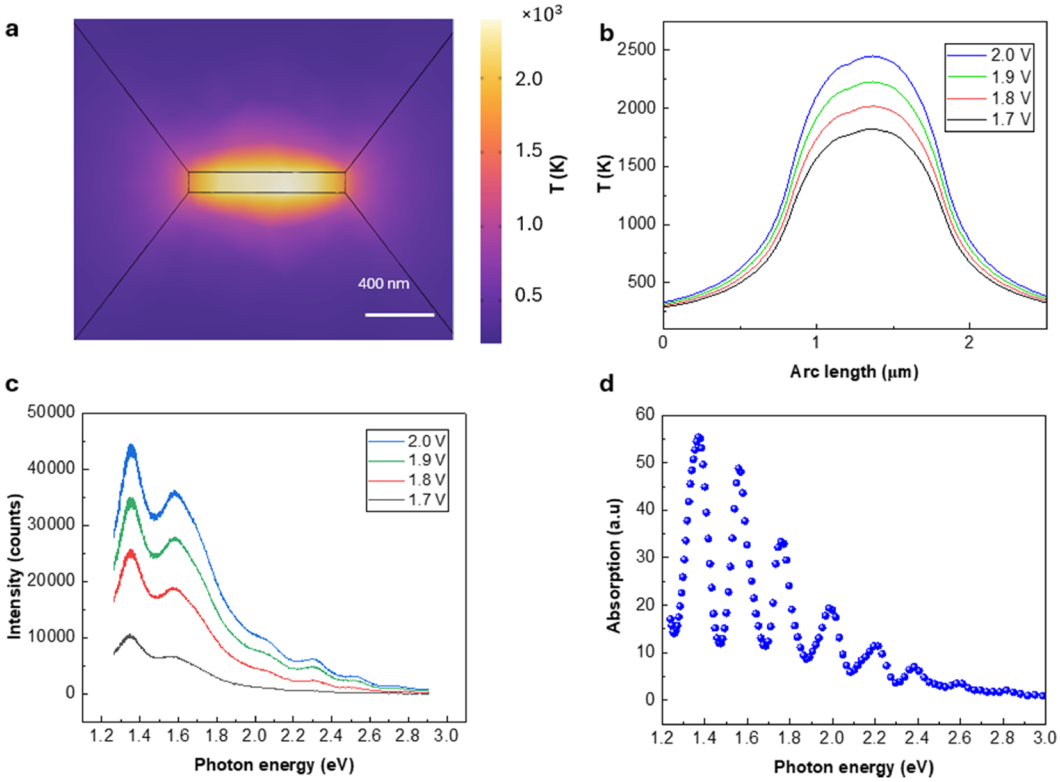

FIG. 4. (a) Simulated temperature map of a Joule-heated TiN NW 1000 nm long and 120 nm wide at a dc bias of 2.0 V. The center of the NW has the highest temperature. (b) Calculated temperature profiles along the centerline of the Joule-heated TiN NW for different dc biases. (c) Measured thermal emission at different bias voltages as a function of photon energy. (d) Calculated absorption for incident plane waves on a TiN NW as a function of incident photon energy, with the photon energy distribution set by a Boltzmann factor with a temperature of 2500 K, for comparison with (c), with interference fringes readily apparent in the absorption. Note that absorption of thermally distributed plane waves is not the inverse of the thermal emission process.

NW length and saturates at around 180 K toward the ends of the electrode contacts, leaving the highest temperature light emission confined to the constriction. In several studies of nanoscale light-emitting devices based on other plasmonic materials, it is common for the electron and lattice temperatures to differ significantly.[41,42] However, TiN is unique in this regard. Its strong electron–phonon coupling at elevated temperatures ensures that it is reasonable to consider the electrons and lattice to have well-defined effective temperatures that are essentially identical. A similar analysis was performed previously for nanowires fabricated from Pt thin films.[30]

Figure 4(c) shows the raw emission spectrum (corrected for wavelength-dependent detector sensitivity) of a resistively heated TiN nanowire at several biases. The oscillating component of the spectrum is an interference effect that originates from the TiN nanowires sitting on a 2 μm-thick SiO_2 layer on the Si substrate. Interference between light directly emitted from the nanowire and light that bounces off the SiO_2/Si interface before reaching the objective leads to the observed minima and maxima as a function of photon energy. Figure 4(d) demonstrates this with a very simple model that approximates the reciprocal process. The model calculates the absorption of transversely polarized (with respect to the wire) plane wave light at various frequencies by an infinitely long TiN nanowire of the appropriate width and thickness on 2 μm-thick SiO_2 on semi-infinite Si as a function of incident photon energy. Scaling the intensity of the incident plane waves by a Boltzmann factor $e^{\frac{-\hbar\omega}{k_B T_{eff}}}$, with an effective temperature of 2500 K, gives a good resemblance to the actual measured emission, with fringes appearing near the experimentally determined energies. The greater depth of the fringes in the model than in the experiment stems from the fact that the plane wave absorption calculation is not actually a true inverse of the thermal emission from a small, nonuniformly radiating nanostructure. We note that thermal emission from plasmon-hosting nanostructures typically has interesting polarization dependence;[43,44] however, for the examined wavelength regime, we do not see signatures of polarization in the emitted light of our biased nanowires. This is possibly due to the comparatively broad plasmon resonances in these films, with plasmon width attributed to the disorder from the polycrystalline nature of the material. This is consistent with the measured AR, which is smaller than the theoretically expected AR by a factor of about 4.

We employ a normalization procedure similar to that employed when examining electroluminescence from nanogap tunnel junctions[45,46] (see the supplementary material). Normalization

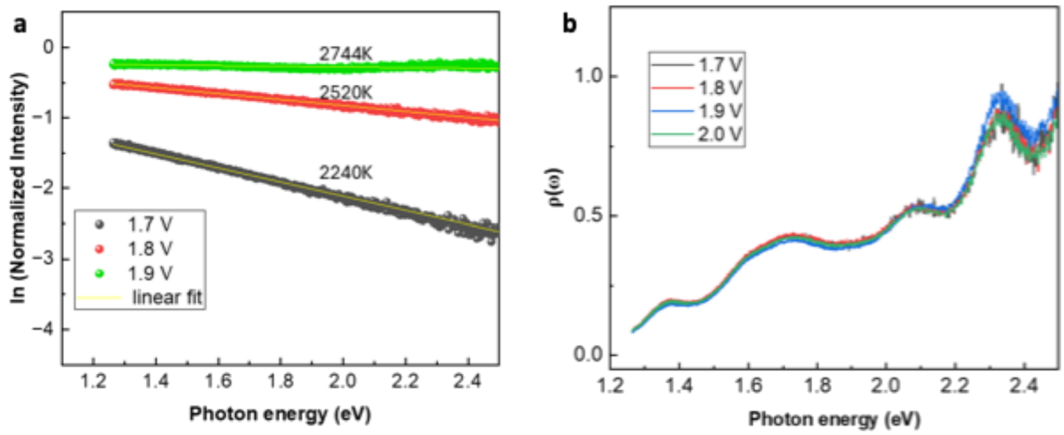

FIG. 5. (a) Energy dependence of the thermal emission spectra from the TiN nanowires obtained by dividing the spectra obtained at 1.7, 1.8, and 1.9 V by the reference spectra taken at 2.0 V, normalizing out the effective energy-dependent spectral emission shape ρ(ω) that includes substrate interference effects. (b) Extracted ρ(ω) for the thermal emission, showing that the spectra in Fig. 4(c) all have the same underlying form.

allows analysis of the emission spectrum's energy dependence while ideally removing the effects of the interference fringes. Figure 5 shows the resulting Boltzmann-like energy dependence once the structural-spectral features are normalized away. Effective temperatures from this analysis at different biases are found and are comparable with the expectations from the thermal model of Fig. 4(b). The voltage-independent ρ(ω) [Fig. 5(b)] shows that all the spectra in Fig. 4(c) have the same underlying structure and implies that the normalization analysis is quantitatively reasonable. The ρ(ω) combines the structural interference effects, the energy-dependent emissivity of the TiN, the photonic density of states for emission, and the collection efficiency of the optical setup. Temperatures from this analysis essentially agree with those calculated from our appropriate finite-element heating models, which supports our interpretation of the origin of the thermal emission, which is the black body emission of electrons in near-thermal equilibrium with the phonons. Our analysis implies that the effective temperature of emitting electrons is approximately directly proportional to the applied bias. This is somewhat counterintuitive, as one might expect temperature elevation to be directly proportional to the dissipated power ($\sim V^2$). However, a quadratic bias dependence neglects the temperature-dependent thermal properties of the nanowire and environment and the fact that the temperature excursion from the environmental 180 K is large. In practice, assuming a quadratic dependence on bias fails to fit the data, suggesting that the temperature dependence of the thermal path is important in the Joule heating luminescence regime.

CONCLUSION

Individual titanium nitride nanowires were studied in the scope of plasmonic heating. Both FEM simulations and heating experiments suggest that TiN NWs can perform as photothermal heaters with significant polarization dependence when illuminated with resonant photon energy. This polarization dependence can be tuned by altering the NW's geometry, which affects the spectral match between the dipolar plasmon resonance and illuminating photon energy. The nanostructures demonstrate promising platforms for bolometric devices based on resistance changes and photothermoelectric response and for developing future nano-photonic technologies and energy conversion devices. This work also demonstrates electrically biased titanium nitride nanowires as nanoscale thermal emitters and light sources. The lithographically designed nanowires ensure high current densities and enhanced Joule heating, leading to electron and lattice temperatures that greatly exceed ambient substrate conditions. The hot nanowire's electrons emit visible light, leaving the other parts of the device non-illuminating. The thermal emission is electrically tunable by changing the applied bias. These results are proof of concept for developing refractory plasmonic and on-chip light sources.

SUPPLEMENTARY MATERIAL

The supplementary material contains a discussion of a finite element model of the photothermal voltage as a function of laser spot position, additional plots showing the polarization-dependent photothermal response of TiN wires, and a summary of the effective temperature analysis of the thermal radiation from the Joule heated wires.

ACKNOWLEDGMENTS

D.N., K.W.S., and S.L. acknowledge the support from the National Science Foundation (NSF) under Award No. ECCS-2309941 and Robert A. Welch Foundation Grant Nos. C-1636 and C-2252. K.P., V.M.S., and A.B. acknowledge the National Science Foundation under the DMREF Award No. 10002504.

AUTHOR DECLARATIONS

Conflict of Interest

The authors have no conflicts to disclose.

Author Contributions

Ken W. Ssennyimba: Data curation (equal); Formal analysis (equal); Investigation (lead); Methodology (equal); Writing – original draft (lead); Writing – review & editing (equal). **Shusen Liao**: Formal analysis (supporting); Methodology (supporting); Writing – review & editing (supporting). **Yunxuan Zhu**: Formal analysis (supporting); Methodology (supporting); Writing – review & editing (supporting). **Tanner J. Legvold**: Methodology (supporting); Writing – review & editing (supporting). **Dale T. Lowder**: Methodology (supporting); Writing – review & editing (supporting). **Karthik Pagadala**: Investigation (supporting); Resources (equal); Writing – review & editing (supporting). **Alexandra Boltasseva**: Funding acquisition (equal); Methodology (supporting); Project administration (supporting); Resources (equal); Supervision (equal); Writing – review & editing (supporting). **Vladimir M. Shalaev**: Funding acquisition (equal); Resources (equal); Writing – review & editing (supporting). **Douglas Natelson**: Conceptualization (lead); Funding acquisition (equal); Project administration (equal); Resources (equal); Supervision (equal); Writing – review & editing (equal).

DATA AVAILABILITY

The data that support the findings of this study are openly available in Zenodo at https://doi.org/10.5281/zenodo.15236899.[44]

REFERENCES

[1] Z. Wang, M. Wang, X. Wang, Z. Hao, S. Han, T. Wang, and H. Zhang, "Photothermal-based nanomaterials and photothermal-sensing: An overview," Biosens. Bioelectron. **220**, 114883 (2023).

[2] A. Badir, S. Refki, and Z. Sekkat, "Utilizing gold nanoparticles in plasmonic photothermal therapy for cancer treatment," Heliyon **11**(4), e42738 (2025).

[3] S. Luo, X. Ren, H. Lin, H. Song, and J. Ye, "Plasmonic photothermal catalysis for solar-to-fuel conversion: Current status and prospects," Chem. Sci. **12**(16), 5701–5719 (2021).

[4] A. Mishra and P. Bäuerle, "Small molecule organic semiconductors on the move: Promises for future solar energy technology," Angew. Chem., Int. Ed. **51**(9), 2020–2067 (2012).

[5] X. Cui, Q. Ruan, X. Zhuo, X. Xia, J. Hu, R. Fu, Y. Li, J. Wang, and H. Xu, "Photothermal nanomaterials: A powerful light-to-heat converter," Chem. Rev. **123**(11), 6891–6952 (2023).

[6] X. Huang, W. Zhang, G. Guan, G. Song, R. Zou, and J. Hu, "Design and functionalization of the NIR-responsive photothermal semiconductor nanomaterials for cancer theranostics," Acc. Chem. Res. **50**(10), 2529–2538 (2017).

[7] J. J. Mock, M. Barbic, D. R. Smith, D. A. Schultz, and S. Schultz, "Shape effects in plasmon resonance of individual colloidal silver nanoparticles," J. Chem. Phys. **116**(15), 6755–6759 (2002).

[8] P. Albella, B. Garcia-Cueto, F. González, F. Moreno, P. C. Wu, T.-H. Kim, A. Brown, Y. Yang, H. O. Everitt, and G. Videen, "Shape matters: Plasmonic nanoparticle shape enhances interaction with dielectric substrate," Nano Lett. **11**(9), 3531–3537 (2011).

[9] P. K. Venuthurumilli, P. D. Ye, and X. Xu, "Plasmonic resonance enhanced polarization-sensitive photodetection by black phosphorus in near infrared," ACS Nano **12**(5), 4861–4867 (2018).

[10] A. Ricciardi, M. Consales, G. Quero, A. Crescitelli, E. Esposito, and A. Cusano, "Versatile optical fiber nanoprobes: From plasmonic biosensors to polarization-sensitive devices," ACS Photonics **1**(1), 69–78 (2014).

[11] P. Zolotavin, A. Alabastri, P. Nordlander, and D. Natelson, "Plasmonic heating in Au nanowires at low temperatures: The role of thermal boundary resistance," ACS Nano **10**(7), 6972–6979 (2016).

[12] H. Takeya, J. Frame, T. Tanaka, Y. Urade, X. Fang, and W. Kubo, "Bolometric photodetection using plasmon-assisted resistivity change in vanadium dioxide," Sci. Rep. **8**(1), 12764 (2018).

[13] A. Hamouleh-Alipour, A. Mir, and A. Farmani, "Design and analytical evaluation of a high resistance sensitivity bolometer sensor based on plasmonic metasurface structure," IEEE J. Sel. Top. Quantum Electron. **28**(2), 1–7 (2022).

[14] P. Zolotavin, C. Evans, and D. Natelson, "Photothermoelectric effects and large photovoltages in plasmonic Au nanowires with nanogaps," J. Phys. Chem. Lett. **8**(8), 1739–1744 (2017).

[15] X. Lu, L. Sun, P. Jiang, and X. Bao, "Progress of photodetectors based on the photothermoelectric effect," Adv. Mater. **31**(50), 1902044 (2019).

[16] M. Dai, C. Wang, B. Qiang, Y. Jin, M. Ye, F. Wang, F. Sun, X. Zhang, Y. Luo, and Q. J. Wang, "Long-wave infrared photothermoelectric detectors with ultrahigh polarization sensitivity," Nat. Commun. **14**(1), 3421 (2023).

[17] K. W. Tan, C. M. Yap, Z. Zheng, C. Y. Haw, P. S. Khiew, and W. S. Chiu, "State-of-the-art advances, development, and challenges of metal oxide semiconductor nanomaterials for photothermal solar steam generation," Adv. Sustainable Syst. **6**(4), 2100416 (2022).

[18] H. Ge, Y. Kuwahara, and H. Yamashita, "Development of defective molybdenum oxides for photocatalysis, thermal catalysis, and photothermal catalysis," Chem. Commun. **58**(61), 8466–8479 (2022).

[19] C. Wang, W. Dong, A. Li, D. G. Atinafu, G. Wang, and Y. Lu, "The reinforced photothermal effect of conjugated dye/graphene oxide-based phase change materials: Fluorescence resonance energy transfer and applications in solar-thermal energy storage," Chem. Eng. J. **428**, 130605 (2022).

[20] G. V. Naik, J. L. Schroeder, X. Ni, A. V. Kildishev, T. D. Sands, and A. Boltasseva, "Titanium nitride as a plasmonic material for visible and near-infrared wavelengths," Opt. Mater. Express **2**(4), 478–489 (2012).

[21] W.-P. Guo, R. Mishra, C.-W. Cheng, B.-H. Wu, L.-J. Chen, M.-T. Lin, and S. Gwo, "Titanium nitride epitaxial films as a plasmonic material platform: Alternative to gold," ACS Photonics **6**(8), 1848–1854 (2019).

[22] K. Polakova, S. Rej, S. Hradilova, J. Belza, T. Malina, K. B. Tomankova, R. Vecerova, P. Matous, P. Paral, A. Opletalova, J. Soukupova, T. Pluhacek, L. Sefc, R. Zboril, S. Kment, and A. Naldoni, "Morphology-dependent near-infrared photothermal activity of plasmonic TiN nanobars and nanospheres for anticancer, antibacterial therapy and deep *in vivo* photoacoustic imaging," Appl. Surf. Sci. Adv. **26**, 100713 (2025).

[23] J. Bi, R. Zhang, X. Yao, and Y. Cao, "The rise of refractory transition-metal nitride films for advanced electronics and plasmonics," Adv. Mater. Interfaces **12**, 2500116 (2025).

[24] K. S. Schramke, Y. Qin, J. T. Held, K. A. Mkhoyan, and U. R. Kortshagen, "Nonthermal plasma synthesis of titanium nitride nanocrystals with plasmon resonances at near-infrared wavelengths relevant to photothermal therapy," ACS Appl. Nano Mater. **1**(6), 2869–2876 (2018).

[25] Z. Liu, G. Liu, Z. Huang, X. Liu, and G. Fu, "Ultra-broadband perfect solar absorber by an ultra-thin refractory titanium nitride meta-surface," Sol. Energy Mater. Sol. Cells **179**, 346–352 (2018).

[26] R. Mishra, C.-W. Chang, A. Dubey, Z.-Y. Chiao, T.-J. Yen, H. W. Howard Lee, Y.-J. Lu, and S. Gwo, "Optimized titanium nitride epitaxial film for refractory plasmonics and solar energy harvesting," J. Phys. Chem. C **125**(24), 13658–13665 (2021).

[27] W. Tao, Y. Hong, J. Sun, Y. Lian, F. Zhou, and L. Jiang, "Ultrafast dynamics and mechanism of structure formation in titanium nitride upon femtosecond laser irradiation for plasmonic enhanced photothermal effect," Surf. Interfaces **52**, 104905 (2024).

[28] S. Rotta Loria, B. R. Bricchi, A. Schirato, L. Mascaretti, C. Mancarella, A. Naldoni, A. Li Bassi, G. Della Valle, and M. Zavelani-Rossi, "Unfolding the origin of the ultrafast optical response of titanium nitride," Adv. Opt. Mater. **11**(15), 2300333 (2023).

[29] D. Benner, J. Boneberg, P. Nürnberger, R. Waitz, P. Leiderer, and E. Scheer, "Lateral and temporal dependence of the transport through an atomic gold contact under light irradiation: Signature of propagating surface plasmon polaritons," Nano Lett. **14**(9), 5218–5223 (2014).

[30]D. R. Ward, N. J. Halas, and D. Natelson, "Localized heating in nanoscale Pt constrictions measured using blackbody radiation emission," Appl. Phys. Lett. **93**(21), 213108 (2008).
[31]M. Roy, N. R. Mucha, S. Fialkova, and D. Kumar, "Effect of thickness on metal-to-semiconductor transition in 2-dimensional TiN thin films," AIP Adv. **11**(4), 045204 (2021).
[32]J. B. Herzog, M. W. Knight, and D. Natelson, "Thermoplasmonics: Quantifying plasmonic heating in single nanowires," Nano Lett. **14**(2), 499–503 (2014).
[33]T. Ming, L. Zhao, Z. Yang, H. Chen, L. Sun, J. Wang, and C. Yan, "Strong polarization dependence of plasmon-enhanced fluorescence on single gold nanorods," Nano Lett. **9**(11), 3896–3903 (2009).
[34]G. P. Szakmany, A. O. Orlov, G. H. Bernstein, and W. Porod, "Shape engineering of antenna-coupled single-metal nanothermocouples," Infrared Phys. Technol. **72**, 101–105 (2015).
[35]G. P. Szakmany, A. O. Orlov, G. H. Bernstein, and W. Porod, "Single-metal nanoscale thermocouples," IEEE Trans. Nanotechnol. **13**(6), 1234–1239 (2014).
[36]H. Liang, J. Xu, D. Zhou, X. Sun, S. Chu, and Y. Bai, "Thickness dependent microstructural and electrical properties of TiN thin films prepared by DC reactive magnetron sputtering," Ceram. Int. **42**(2), 2642–2647 (2016).
[37]M. Jonson and G. D. Mahan, "Mott's formula for the thermopower and the Wiedemann-Franz law," Phys. Rev. B **21**(10), 4223–4229 (1980).
[38]P. Zolotavin, C. I. Evans, and D. Natelson, "Substantial local variation of the Seebeck coefficient in gold nanowires," Nanoscale **9**(26), 9160–9166 (2017).
[39]C. I. Evans, R. Yang, L. T. Gan, M. Abbasi, X. Wang, R. Traylor, J. A. Fan, and D. Natelson, "Thermoelectric response from grain boundaries and lattice distortions in crystalline gold devices," Proc. Natl. Acad. Sci. U. S. A. **117**(38), 23350–23355 (2020).
[40]R. Machunze and G. C. A. M. Janssen, "Stress and strain in titanium nitride thin films," Thin Solid Films **517**(20), 5888–5893 (2009).
[41]Y. D. Kim, H. Kim, Y. Cho, J. H. Ryoo, C.-H. Park, P. Kim, Y. S. Kim, S. Lee, Y. Li, S.-N. Park, Y. Shim Yoo, D. Yoon, V. E. Dorgan, E. Pop, T. F. Heinz, J. Hone, S.-H. Chun, H. Cheong, S. W. Lee, M.-H. Bae, and Y. D. Park, "Bright visible light emission from graphene," Nat. Nanotechnol. **10**(8), 676–681 (2015).
[42]A. Downes, P. Dumas, and M. E. Welland, "Measurement of high electron temperatures in single atom metal point contacts by light emission," Appl. Phys. Lett. **81**(7), 1252–1254 (2002).
[43]L. J. Klein, S. Ingvarsson, and H. F. Hamann, "Changing the emission of polarized thermal radiation from metallic nanoheaters," Opt. Express **17**(20), 17963–17969 (2009).
[44]P.-E. Chang, Y.-W. Jiang, H.-H. Chen, Y.-T. Chang, Y.-T. Wu, L. D.-C. Tzuang, Y.-H. Ye, and S.-C. Lee, "Wavelength selective plasmonic thermal emitter by polarization utilizing Fabry-Pérot type resonances," Appl. Phys. Lett. **98**(7), 073111 (2011).
[45]M. Buret, A. V. Uskov, J. Dellinger, N. Cazier, M.-M. Mennemanteuil, J. Berthelot, I. V. Smetanin, I. E. Protsenko, G. Colas-des-Francs, and A. Bouhelier, "Spontaneous hot-electron light emission from electron-fed optical antennas," Nano Lett. **15**(9), 5811–5818 (2015).
[46]L. Cui, Y. Zhu, M. Abbasi, A. Ahmadivand, B. Gerislioglu, P. Nordlander, and D. Natelson, "Electrically driven hot-carrier generation and above-threshold light emission in plasmonic tunnel junctions," Nano Lett. **20**(8), 6067–6075 (2020).